Testing and Analysis of Steel and Concrete Beam-Column Assemblies under a Column Removal Scenario

Fahim Sadek, M.ASCE[1]; Joseph A. Main, A.M.ASCE[2]; H.S. Lew, F.ASCE[3]; and Yihai Bao[4]

Abstract: This paper presents an experimental and computational assessment of the performance of steel and reinforced concrete beam-column assemblies under monotonic vertical displacement of a center column, simulating a column removal scenario. The assemblies represent portions of structural framing systems designed as Intermediate Moment Frames (IMFs) and Special Moment Frames (SMFs), for Seismic Design Categories C and D, respectively. The steel IMF and SMF assemblies were designed in accordance with ANSI/AISC 341-02 using prequalified moment connections specified in FEMA 350. The concrete IMF and SMF assemblies were designed and detailed in accordance with ACI 318-02 requirements. Each full-scale assembly comprises two beam spans and three columns, and downward displacements of the center column are imposed until failure. The study provides insight into the behavior and failure modes of the assemblies, including the development of catenary action. Both detailed and reduced finite element models are developed, which capture the primary response characteristics and failure modes. Analyses with the reduced models can be executed rapidly without loss of accuracy, facilitating implementation in models of entire structural systems.

CE Database subject headings: Buildings; Concrete structures; Finite element method; Full-scale tests; Nonlinear analysis; Progressive collapse; Seismic design; Steel structures.

[1] Leader, Structures Group, National Institute of Standards and Technology, Gaithersburg, MD 20899-8611. E-mail: fahim.sadek@nist.gov
[2] Research Structural Engineer, National Institute of Standards and Technology, Gaithersburg, MD 20899-8611 (corresponding author). E-mail: joseph.main@nist.gov
[3] Senior Research Structural Engineer, National Institute of Standards and Technology, Gaithersburg, MD 20899-8611. E-mail: hai.lew@nist.gov
[4] Guest Researcher, National Institute of Standards and Technology, Gaithersburg, MD 20899-8611. E-mail: yihai.bao@nist.gov

Introduction

Since the destruction of the Alfred P. Murrah Federal Building in 1995, caused by a truck bomb attack (FEMA 1996), and the collapse of the World Trade Center towers in 2001, caused by the impact of large passenger jetliners (NIST 2005), the engineering community, including codes and standards development organizations and public regulatory agencies, has paid greater attention to the performance of buildings subjected to damage from abnormal events. In the U.S., the American Society of Civil Engineers Standard 7 (ASCE 2010, Section C1.4), and the guidelines of the U.S. General Services Administration (GSA 2003) and the Department of Defense (DOD 2009) provide guidance to prevent disproportionate collapse (also known as progressive collapse). Disproportionate collapse occurs when an initial local failure spreads progressively, resulting in total collapse or collapse of a disproportionately large part of a structure. Resistance to disproportionate collapse is achieved either implicitly, by providing minimum levels of strength, continuity, and ductility; or explicitly, by (1) providing alternate load paths so that local damage is absorbed and major collapse is averted or (2) providing sufficient strength to structural members that are critical to global stability.

In the alternate path method, structural integrity is assessed through analysis, to ascertain whether the structural system can bridge over failed structural members. For example, if a column is damaged, continuity of the beams adjacent to the top of the damaged column is required to redistribute the loads previously carried by the damaged column. The analysis must demonstrate the adequacy of the beams and their connections to redistribute these loads, potentially through catenary action. An accurate characterization of the nonlinear, large-deformation behavior associated with the transfer of forces through the connections in such scenarios is critical in assessing the potential for disproportionate collapse. Physical tests are indispensible in validating the analytical models used to represent nonlinear connection behavior in such scenarios.

This paper describes both full-scale testing and finite element-based modeling of four beam-column assemblies, including two steel assemblies and two reinforced concrete assemblies. Each assembly comprises three columns and two beams, representing a portion of the second floor framing of a prototype ten-story building. While both steel assemblies have moment resisting beam-to-column connections, one assembly represents a portion of an intermediate moment frame (IMF) designed for Seismic Design Category C (SDC C) and the other represents a portion of a special moment frame (SMF) designed for SDC D. Similarly, one concrete assembly represents a portion of an IMF and the other represents a portion of an SMF. These assemblies are referred to subsequently as the IMF assembly and the SMF assembly, respectively.

The beam-column assemblies are subjected to monotonically increasing vertical displacement of the unsupported center column to observe their behavior under a simulated column removal scenario, including the development of catenary action in the beams. Each test is continued until a collapse mechanism of the assembly is reached. Both detailed and reduced finite element models of the test specimens are developed, and the model predictions show good agreement with the experimental results, providing validation of the modeling approaches. The reduced models can be used for analysis of complete structural systems to assess their vulnerability to disproportionate collapse. The tests and associated computational models help fill the gap in defining the response characteristics of the moment-resisting connections under collapse scenarios and contribute to establishing a library of validated connection models that can be used to assess the robustness of structural systems.

Description of Building Designs

The ten-story prototype buildings have rectangular plan dimensions of 30.5 m by 45.7 m. For both the steel and concrete prototype buildings, alternate designs were developed for SDC C and for SDC D. This was done to examine the effectiveness of seismic design and detailing on

disproportionate collapse resistance. In this study, moment-resisting frames are considered for the lateral force-resisting system.

Steel Frame Buildings

The steel prototype buildings were designed and detailed in accordance with the American Institute Steel of Construction Seismic Provisions, ANSI/AISC 341-02 (AISC 2002). The buildings used moment frames at the perimeter for the lateral-load resisting system, with gravity frames on the interior. Connections used in the moment frames were selected from the prequalified steel connections specified in FEMA 350 (FEMA 2000a): (1) welded unreinforced flange-bolted web (WUF-B) connections for the IMFs (SDC C), and (2) Reduced Beam Section (RBS) connections for the SMFs (SDC D). ASTM A992 structural steel (F_y = 345 MPa) was used for all beams, columns, and doubler plates in the panel zones. ASTM A36 steel (F_y = 248 MPa) was used for the shear tabs and continuity plates at the beam-to-column joints. ASTM A490 high strength bolts were used for the bolted connections, and welding requirements followed the recommendations in FEMA 353 (FEMA 2000b).

Concrete Frame Buildings

The concrete prototype buildings were designed and detailed in accordance with the American Concrete Institute's Building Code Requirements for Structural Concrete, ACI 318-02 (ACI 2002). Both the SDC C and SDC D buildings were designed using normal weight concrete having a specified compressive strength of 27.6 MPa and reinforcing steel of ASTM A615 having a minimum specified yield strength of 414 MPa.

Steel Beam-Column Assemblies

A schematic of the test setup for the steel beam-column assemblies is shown in Fig. 1. The same experimental setup was used for the SMF and IMF assembly tests, with some differences in the instrumentation layout. Details of the beam-to-column connections used in the IMF and SMF assemblies are shown in Figs. 2(a) and 2(b), respectively. Fig. 3 shows photographs of the steel IMF assembly, including a close-up view of the connections to the center column.

The bases of the exterior columns were anchored to the strong floor of the test facility, and the top of each exterior column was rigidly attached to two diagonal braces to restrain horizontal movement. The base of the center stub column was unrestrained vertically, but out-of-plane movement was restrained. In addition, the beams were restrained from out-of-plane movement at mid-span by lateral bracing. A hydraulic actuator with a capacity of 2670 kN and stroke of 508 mm was attached to the top of the center column to apply a vertical load to the specimen. Load was applied under displacement control at a rate of 25 mm/min. The uncertainty in the measured data from the load cells, deflection gages, strain gages, and inclinometers was within ±1 %.

The following sections present test results for the steel IMF and SMF assemblies and describe finite element models of these assemblies. Further details on the test program, experimental results, and finite element models are provided in Sadek et al. (2010).

Steel IMF Assembly

The steel IMF assembly comprised two W21x73 beams connected to three W18x119 columns by WUF-B connections. The span length of the beams (center-to-center of columns) was 6.10 m. The WUF-B connection is similar to the connection commonly used prior to the 1994 Northridge earthquake. FEMA 355D (FEMA 2000c) provides extensive information on testing and performance of WUF-B connections under cyclic loading.

Details of the WUF-B connection used in the IMF assembly are shown in Fig. 2(a). The beam web is connected to the column flange using a shear plate (shear tab), which is welded to the column using an 8 mm fillet weld and bolted to the beam web using three 25 mm diameter ASTM A490 bolts. The bolt holes are standard holes with an edge distance of 70 mm. The beam flanges are joined to the column flange using complete joint penetration (CJP) groove welds. Weld access holes are cut from the beam flanges according to the recommendations of FEMA 350 (FEMA 2000a). Continuity plates are provided for both center and exterior columns as shown in Fig. 2(a). No doubler plates were required.

Test Results

Under monotonic vertical displacement of the center column, the assembly experienced large deflections and rotations prior to failure. The connection failed at a vertical displacement of the center column of about 495 mm. At that displacement, the applied vertical load was about 890 kN. The connection failed in the following sequence (see Fig. 4): (1) local buckling of the top flanges of the beams at the center column, (2) successive shear fractures of the lowermost and middle bolts connecting the beam web to the shear tab, and (3) fracture of the bottom flange near the weld access hole.

Plots of the applied vertical load versus vertical displacement of the center column and the beam axial force versus the vertical displacement of the center column are shown in Fig. 5. Experimental measurements are presented along with finite element model predictions that will be discussed subsequently. The experimental beam axial force is calculated based on measured strains in the beams. As the plots indicate, the assembly was unloaded at a vertical displacement of about 460 mm, to adjust the stroke of the hydraulic ram, and was then reloaded to failure. Fig. 5(a) indicates that the assembly remained in the elastic range up to a vertical displacement of the center column of about 50 mm. In the early stages of loading, the behavior of the assembly was primarily flexural, with compressive axial forces in the beams, shown in Fig. 5(b), associated

with frame action of the assembly. As the loading progressed, with increased vertical displacement of the center column, the response of the assembly was dominated by catenary action, as indicated by the development of axial tension in the beams shown in Fig. 5(b). At the time of failure, the axial tension in the beams was about 667 kN.

Finite Element Models

Two finite element models of the steel IMF assembly were developed to study the behavior of the connections and to compare the calculated response with experimental values. The first was a detailed model of the assembly with approximately 300 000 elements, while the second was a reduced model with about 150 elements. The analyses were conducted using explicit time integration in the LS-DYNA finite element software package (Hallquist 2007). Overviews of both models are shown in Fig. 6.

The detailed model, shown in Fig. 6(a), consisted of finely meshed solid elements representing the beams, columns, continuity plates, shear tabs, bolts, and welds in the vicinity of the connection. Contact was defined between the bolts, shear tabs, and beam webs to model the transfer of forces through the bolted connection, including friction and bolt bearing. Away from the connection zones, the beams and columns were modeled with shell elements. Spring elements were used to model the diagonal braces attached to the tops of the exterior columns, with a nonlinear load-displacement behavior based on measured displacement and force values (Sadek et al. 2010). All nodes were fixed at the bases of the exterior columns. In order to reduce the time required for computation, only half of the assembly was modeled, and symmetry boundary conditions were enforced along the plane of symmetry through the center column. The steel for the various components was modeled using a piecewise-linear plasticity model (material 24 in LS-DYNA), with stress-strain curves based on coupon test data obtained for all steel sections and plates. Fracture was modeled using element erosion, in which elements were deleted from the model at a specified value of the effective plastic strain. Values of erosion strain were

calibrated to match failure strain values from tensile tests using models of the tensile coupons. Because of mesh size sensitivity in the modeling of necking behavior, larger values of the erosion strain were required in regions with smaller elements (Sadek et al. 2010).

The reduced model used Hughes-Liu beam elements with cross-section integration (Hallquist 2007) to model the beams and columns, as well as the shear tabs and beam flanges in the connection regions. The steel was modeled using a piecewise-linear plasticity model (material 24 in LS-DYNA) based on coupon test data. Fracture was modeled using element erosion, with values of erosion strain for a particular element size calibrated for consistency with tensile coupon test results. An arrangement of beam and spring elements, connected with rigid links, was used to model the WUF-B connection as shown in Fig. 6(b). Nonlinear spring elements were used to model the shear behavior of the bolts, along with bearing-induced deformations of the shear tab and beam web. The shear load-deformation curve used for these spring elements was based on the results of a detailed solid-element model of the bolted connection (Sadek et al. 2010). Nonlinear spring elements were also used to model the diagonal braces and the shear behavior of the panel zone. For the panel zone, the diagonal springs had an elasto-plastic load deformation curve based on the geometry and strength of the panel zone (Sadek et al. 2010). Two analyses were conducted in which the bases of the exterior columns were modeled as either fixed or pinned.

Based on the analysis of the detailed model, the beam-column assembly responded initially in a purely flexural mode before catenary action developed. The beam remained essentially elastic except for the sections in the vicinity of its connections, where significant yielding was observed. The failure mode of the connection based on this analysis, shown in Fig. 7, was very similar to that observed in the experiment (Fig. 4). The results from the reduced model were consistent with those from the detailed model.

In Fig. 5 comparisons are presented between the finite element model predictions and the experimental measurements of (a) the vertical load and (b) the beam axial force, plotted against

the vertical displacement of the center column. The plots indicate good agreement between the experimental and computational results using both the detailed and reduced models.

Steel SMF Assembly

Due to the similarities between the test layout, boundary conditions, and loading system of the IMF and SMF assemblies, only a brief overview of the steel SMF assembly is presented herein. The reader is referred to Sadek et al. (2010) for further details.

The SMF assembly comprised two W24x94 beams connected to three W24x131 columns by RBS connections. The overall dimensions of the SMF assembly were the same as those of the IMF assembly. The RBS connections used in the SMF assembly are created by cutting away a portion of the top and bottom flanges of the beam at a distance from the beam-column interface so that yielding would be concentrated in this reduced area. The RBS connection was developed as a result of extensive research following the 1994 Northridge earthquake and has been used for seismic design since then. FEMA 355D (FEMA 2000c) provides extensive information on testing and performance of RBS connections under cyclic loading.

Details of the RBS connection used in the SMF assembly are shown in Fig. 2(b). As shown in the figure, the beam flanges and web are connected to the column flange using CJP groove welds. The connection is created by circular radius cuts in both top and bottom flanges of the beam. Continuity plates are provided for both center and exterior columns, while doubler plates were required only for the center column.

Test Results

The connection failed at a vertical displacement of the center column of about 850 mm. At that displacement, the applied vertical load was about 1780 kN. The failure was characterized by fracture of the bottom flange in the middle of the reduced section of one of the connections near

the center column. The fracture propagated through the web, as shown in Fig. 8, until the vertical load-carrying capacity of the assembly was depleted.

Plots of (a) the vertical load and (b) the beam axial force versus the vertical displacement of the center column are shown in Fig. 9. Also shown are the predictions of finite element models, which are discussed subsequently. The experimental beam axial force is calculated based on measured strains in the beams. As the plots indicate, the specimen was unloaded at vertical displacements of about 440 mm and 840 mm, to adjust the stroke of the hydraulic ram, and was then reloaded to failure. Similar to the IMF assembly, in the early stages of loading, the response of the assembly was primarily flexural. With increased vertical displacement, tensile axial forces developed in the beams, as shown in Fig. 9(b), and the behavior was dominated by catenary action. At the time of failure, the axial tension in the beams was about 2450 kN.

Finite Element Models

Similar to the IMF assembly, two finite element models were used to calculate the response of the SMF assembly. The detailed model consisted of shell elements representing the columns, beams, continuity and doubler plates, and welds. Finer meshes were used in the vicinity of the reduced section. Spring elements were used to model the diagonal braces attached to the tops of the exterior columns, with a nonlinear load-displacement behavior based on measured displacement and force values (Sadek et al. 2010). All nodes were fixed at the bases of the exterior columns. The steel for the various elements was modeled using a piecewise-linear plasticity model based on coupon test data obtained for all steel sections and plates. Fracture was modeled using element erosion, with values of the erosion strain calibrated to match tensile coupon test results. The reduced model consisted of beam and spring elements. Each reduced beam section was modeled using five beam elements with varying section properties. The steel behavior in the reduced model was also represented using a piecewise-linear plasticity model, with fracture modeled using element erosion. Nonlinear spring elements were used to model the diagonal

braces and the shear behavior of the panel zone. Both fixed and pinned bases were considered for the exterior columns.

The detailed model showed that the beam-column assembly responded initially in a flexural mode before catenary action developed. The failure mode of the assembly, shown in Fig. 10, was very similar to that observed in the experiment (see Fig. 8). The results from the reduced model were consistent with those from the detailed model.

In Fig. 9 comparisons are presented between the finite element model predictions and the experimental measurements of (a) the vertical load and (b) the beam axial force, plotted against the vertical displacement of the center column. Good agreement is observed between the experimental and computational results for both the detailed and reduced models. The plots also indicate that the results using the reduced models with pinned and fixed boundary conditions at the exterior column bases generally bracketed the experimental results.

Concrete Beam-Column Assemblies

A schematic of the test setup used for the concrete beam-column assemblies is shown in Fig. 11. While the dimensions shown in Fig. 11 correspond to the IMF assembly, the experimental setup was identical for the SMF assembly tests. Details of the cross sectional dimensions and reinforcement used in the IMF and SMF assemblies are shown in Fig. 12. A photograph of the SMF assembly in the post-ultimate-load position is shown in Fig. 13.

As shown in Fig. 11, the load was applied to the center stub column by means of four post-tensioning rods that were pulled down by four hydraulic rams, each having a capacity of 534 kN and a stroke of 102 mm. Because this loading scheme is self-centering, lateral bracing of the center stub column was not required. The load was applied under displacement control at a rate of 25 mm/min. The instrumentation used in the concrete assembly tests includes displacement transducers, inclinometers, vertical displacement encoders, Optotrak (a surface position

measuring device) targets, and strain gages, which were cemented to both beam and column reinforcing bars. The uncertainty in the measured data from the load cells was within ± 1 %.

The tops of the exterior columns were restrained from horizontal movement by steel rollers (see Fig. 11), while vertical motion was permitted. The bases of the exterior columns were fixed to large footings which in turn were anchored to the test floor. Both top and bottom longitudinal beam reinforcing bars were spliced with threaded couplers at mid-span of the beams. Mechanical bar couplers were used instead of lap splices in order to evaluate their effectiveness in the development of catenary action. In the U.S., it is not uncommon to use mechanical couplers, particularly for large size bars, to reduce bar congestion and enhance concrete consolidation. Mechanical bar couplers are also used extensively in seismic designs. All longitudinal beam reinforcing bars were anchored at the exterior beam-column joints by means of threaded mechanical anchorage devices supplemented with 19 mm thick steel plates.

The following sections present test results for the concrete IMF and SMF assemblies and describe finite element models of these assemblies. Further details on the test program, experimental results, and finite element models are provided in Lew et al. (2011).

Concrete IMF Assembly

The concrete IMF assembly comprised two 711 mm by 508 mm beams supported by three 711 mm by 711 mm columns as shown in Fig. 12. The span length of the beams (center-to-center of columns) was 6.10 m. The compressive strength of the concrete was 32.4 MPa based on 6 x 12 cylinder tests at the time of testing.

Test Results

Fig. 14(a) shows a plot of the vertical load versus the vertical displacement of the center column. Experimental measurements are presented along with model predictions that will be discussed subsequently. As the load was increased, flexural cracks developed in the tension zones, at the

top of the beams adjacent to the exterior columns and at the bottom of the beams adjacent to the center column. Yielding of the longitudinal reinforcing bars in the cracked regions was first detected at about 267 kN. The load reached an initial peak of 296 kN at a vertical displacement of 127 mm and started to decrease with additional displacement. This decrease in load was associated with crushing of concrete at the top of the beams adjacent to the center column. The load leveled off at 196 kN at a displacement of 406 mm. With further increases in displacement, the load began to increase again due to the development of catenary action, while the cracks at the bottom of the beams near the center column widened. The assembly attained a maximum load of 547 kN at a vertical displacement of 1090 mm, at which point one of the bottom reinforcing bars ruptured, and the load dropped to about half of its maximum value. A second bar ruptured at a displacement of 1130 mm (see Fig. 15).

Finite Element Models

The IMF assembly was modeled using two different approaches: a detailed finite element model with approximately 70 000 elements and a reduced model with about 170 elements. Calculated structural responses were compared to those measured from the experiment. The analyses were conducted using LS-DYNA (Hallquist 2007). Overviews of both models are shown in Fig. 16.

In the detailed model, concrete was represented by finely meshed solid elements and reinforcing bars were modeled as beam elements. A contact interface between beam elements and solid elements was defined to describe the bond-slip behavior of reinforcing bars in the beams. The bottom of the exterior columns was assumed to be fixed. Since the tops of the exterior columns were restrained horizontally by steel rollers (see Fig. 11), contact was defined between the columns and rigid cylinders representing the rollers (not shown in Fig. 16). Steel properties of reinforcing bars were modeled using a piecewise-linear plasticity model with stress-strain curves based on tensile test data. Fracture was modeled using element erosion, with values of erosion strain for a particular element size calibrated to match failure strain values from tensile

tests (Lew et al. 2011). The concrete material was modeled by a continuous surface cap model (material 159 in LS-DYNA). This model (Murray 2007) captures dominant response characteristics of concrete, including confinement effects and softening due to damage accumulation. The model uses a constant fracture energy approach to regulate sensitivity of the results to mesh size, mitigating spurious localization of damage in the modeling of softening behavior.

In the reduced model, the beams and columns were modeled using Hughes-Liu beam elements (Hallquist 2007) with cross-section integration incorporating distinct integration points for the concrete and each reinforcing bar. Similar to the approach used in the detailed model, a constant fracture energy approach was used to limit localization in the modeling of concrete softening. The integration points representing reinforcing bars used a piecewise-linear plasticity model, and fracture was represented using element erosion as explained above. An arrangement of beams, spring elements and rigid links was used to simulate the behavior of beam-column joints [Fig. 16(b)]. Joint shear was represented by rotational springs. Critical sections at the beam-to-column interface were modeled using a beam element with bond-slip effects incorporated into the constitutive model for the reinforcing bars (Lew et al. 2010).

The failure mode predicted by both the detailed and reduced models was fracture of the longitudinal bottom bars of the beams near the center column, as illustrated in Fig. 17 for the detailed model. These predictions were consistent with the failure mode observed in the test (see Fig. 15).

In Fig. 14(a) comparisons are presented between the model predictions and the experimental measurements of the applied vertical load, plotted against the vertical displacement of the center column. Good agreement is observed between the experimental and computational results for both the detailed and reduced models. The plots show that the models are able to correctly predict significant softening after an initial peak load, with subsequent increases in load due to catenary action. Catenary action is indicated by the increasing axial tension evident in Fig. 14(b),

which shows model predictions of the beam axial force versus the vertical displacement of the center column. In the early stages of loading, the beam is predominantly in compression due to arching action, and subsequently the compression force is reduced due to softening and crushing of concrete. As the loading progresses with increased vertical displacement of the center column, the response of the assembly is dominated by catenary action. Further discussion of the different stages of response is provided in Bao (2008).

Concrete SMF Assembly

The concrete SMF assembly comprised two 864 mm by 660 mm beams supported by three 864 mm by 864 mm columns as shown in Fig. 12. The span length (center-to-center of columns) of the beams was 6.10 m. The test setup and instrumentation layout are the same as for the IMF assembly test (see Fig. 11). The compressive strength of the concrete was 35.9 MPa based on 6 x 12 cylinder tests at the time of testing.

Test Results

Fig. 18(a) shows a plot of the vertical load versus the vertical displacement of the center column. Experimental measurements are presented along with finite element model predictions that will be discussed subsequently. The overall behavior of the SMF assembly was similar to that of the IMF assembly wherein an initial flexural behavior was followed by catenary action, which allowed the assembly to attain a higher load as described above. The load reached an initial peak of about 900 kN at a vertical displacement of about 100 mm and started to decrease with additional displacement. Fig. 13 shows the final position of the assembly after reaching a maximum load of 1230 kN at a center column deflection of 1220 mm. Fig. 19 shows the failure mode of the SMF assembly, which was yielding and fracture of a bottom bar adjacent to the center column.

Finite Element Models

The SMF assembly was modeled using both detailed and reduced models, following a similar approach to that used for the IMF assembly. Horizontal slippage of the north column footing was observed and measured during the test, with a maximum value of 19.6 mm. This slippage was incorporated into the numerical models by applying the measured horizontal displacement to the column base. Both models were able to correctly predict the occurrence of the first bottom bar fracture on the side of the center column where the exterior column footing slipped (see Fig. 20).

In Fig. 18(a) comparisons are presented between the model predictions and the experimental measurements of the applied vertical load, plotted against the vertical displacement of the center column. Good agreement is observed between the experimental and computational results for both the detailed and reduced models. Fig. 18(b) shows model predictions of the beam axial force versus the vertical displacement of the center column, in which the development of catenary action is indicated by the increasing axial tension. The curves in Fig. 18 have a similar shape to those of the IMF assembly (see Fig. 14). However, the ultimate load of the SMF assembly is about twice that of the IMF assembly, while the initial peak load of the SMF assembly is about three times that of the IMF assembly. The ratio of the ultimate load to the initial peak load is thus 1.82 for the IMF assembly and 1.37 for the SMF assembly.

Discussion and Conclusions

This paper presented results of both full-scale testing and finite-element based modeling of four beam-column assemblies, including two steel assemblies and two reinforced concrete assemblies. Each assembly comprised three columns and two beams with spans of 6.10 m, and each was subjected to monotonic vertical displacement of the center column until failure, simulating a column removal scenario. The assemblies represented portions of the structural framing systems

of 10-story buildings designed as Intermediate Moment Frames (IMFs) and Special Moment Frames (SMFs), for Seismic Design Categories C and D, respectively.

The steel IMF assembly, which incorporated welded, unreinforced flange, bolted web connections, failed at a vertical column displacement of 495 mm, with a corresponding ultimate load of 890 kN. The steel SMF assembly, which incorporated reduced beam section connections, failed at a vertical column displacement of 850 mm, with a corresponding ultimate load of 1780 kN. It is thus observed that the more stringent seismic design and detailing of the steel SMF assembly increased the failure displacement by a factor of 1.72 and the ultimate load by a factor of 2.00 relative to the steel IMF assembly. The vertical load versus displacement curves of the two steel assemblies exhibited similar characteristics, with an initial linear portion, yielding at a vertical displacement of about 50 mm, and a gradually increasing load beyond yielding until failure. The observed hardening behavior beyond yielding was associated with the development of catenary action, and peak axial tension values of about 670 kN and 2450 kN were measured in the beams of the steel IMF and SMF assemblies, respectively. The failure mechanism of both steel assemblies involved fracture of the bottom flanges of the beams near the connection to the center column.

The concrete IMF assembly failed at a vertical column displacement of 1090 mm, with a corresponding ultimate load of 547 kN. The concrete SMF assembly failed at a vertical column displacement of 1220 mm, with a corresponding ultimate load of 1230 kN. The failure displacements of the two concrete assemblies were thus fairly similar, being only 1.13 times larger for the SMF assembly. The ultimate load of the SMF assembly, however, was 2.25 times larger than that of the IMF assembly, reflecting the more stringent seismic design and detailing of the concrete SMF assembly. The vertical load versus displacement curves of the two concrete assemblies exhibited generally similar characteristics. In contrast with the steel assemblies, the concrete assemblies exhibited softening behavior, with an initial peak load at a vertical displacement of about 100 mm and reductions in load thereafter, up to a displacement of about

500 mm, at which point the load began to increase again up to the point of failure. The observed softening behavior was associated with softening and crushing of concrete, while the subsequent hardening behavior was associated with the development of catenary action. The initial peak load was about 300 kN for the concrete IMF assembly and about 900 kN for the concrete SMF assembly. The ultimate load thus exceeded the initial peak load by a factor of 1.82 for the IMF assembly and 1.37 for the SMF assembly. The failure mechanism of both assemblies involved fracture of the bottom reinforcing bars near the center column.

Both detailed and reduced finite element models of the assemblies were developed, and the computational predictions showed good agreement with the experimentally observed response characteristics and failure modes, providing validation of the modeling approaches. The detailed models involved hundreds of thousands of solid and/or shell elements and were capable of representing the behavior and failure of the assemblies in great detail. The reduced models, which involved on the order of a hundred beam and spring elements, also accurately captured the behavior and failure modes of the assemblies. Analyses with the reduced models can be executed much more rapidly, making the reduced models valuable in the analysis of complete structural systems to assess the reserve capacity and robustness of building structures.

Acknowledgments

The steel assembly tests were carried out at the Engineering Research and Development Center (ERDC) of the U.S. Army Corps of Engineers, Vicksburg, MI, under the supervision of Stephen Robert and Vincent Chiarito. The concrete assembly tests were carried out at the Bowen Laboratory of Purdue University under the direction of Professors Santiago Pujol and Mete Sozen. The steel assembly tests were supported by NIST, ERDC, the Defense Threat Reduction Agency, the U.S. Air Force, and the American Institute of Steel Construction. The concrete assembly tests were supported by NIST and the Department of Homeland Security. Valuable

suggestions and review comments from Professors Sashi Kunnath and Sherif El-Tawil in the development of the numerical models are gratefully acknowledged.

Certain commercial software or materials are identified to describe a procedure or concept adequately. Such identification is not intended to imply recommendation, endorsement, or implication by NIST that the software or materials are necessarily the best available for the purpose.

References

ASCE (2010). *Minimum Design Loads for Buildings and Other Structures, SEI/ASCE 7-10*, American Society of Civil Engineers, Reston, VA.

ACI (2002). *Building Code Requirements for Structural Concrete (ACI 318-02)*, American Concrete Institute, Farmington Hills, MI.

AISC (2002). *Seismic Provisions for Structural Steel Buildings, ANSI/AISC 341-02*, American Institute of Steel Construction, Chicago, IL.

Bao, Y. (2008). *Macromodel-Based Progressive Collapse Simulation of Reinforced Concrete Structures*, Ph.D. Dissertation, University of California, Davis, CA.

DOD (2009). *Design of Buildings to Resist Progressive Collapse, Unified Facilities Criteria (UFC) 4-023-03*, Department of Defense, 25 January 2009.

FEMA (1996). *The Oklahoma City Bombing: Improving building performance through multi-hazard mitigation, FEMA Report 277*, Federal Emergency Management Agency, Washington, D.C.

FEMA (2000a). *Recommended Seismic Design Criteria for New Steel Moment-Frame Buildings, FEMA 350*, SAC Joint Venture and Federal Emergency Management Agency, Washington, D.C.

FEMA (2000b). *Recommended Specifications and Quality Assurance Guidelines for Steel Moment-Frame Construction for Seismic Applications, FEMA 353*, SAC Joint Venture and Federal Emergency Management Agency, Washington, D.C.

FEMA (2000c). *State of the Art Report on Connection Performance, FEMA 355D*, SAC Joint Venture and Federal Emergency Management Agency, Washington, D.C.

FEMA (2000d). *Prestandard and Commentary for the Seismic Rehabilitation of Buildings, FEMA 356*, Federal Emergency Management Agency, Washington, D.C.

GSA (2003). *Progressive Collapse Analysis Design Guidelines for New Federal Office Buildings and Major Modernization Projects*, General Services Administration, Washington, D.C.

Hallquist, J. (2007). *LS-DYNA Keyword User's Manual*, Livermore Software Technology Corporation, Livermore, CA, Version 971.

Lew, H.S., Bao, Y., Sadek, F., Main, J.A., Pujol, S., and Sozen, M.A. (2011). *An Experimental and Computational Study of Reinforced Concrete Assemblies under a Column Removal Scenario*, *NIST Technical Note XXXX*, National Institute of Standards and Technology, Gaithersburg, MD.

Murray, Y.D. (2007). *Users Manual for LS-DYNA Concrete Material Model 159, FHWA-HRT-05-062*, Federal Highway Administration, McLean, VA.

NIST (2005). *The Collapse of the World Trade Center Towers, NIST NCSTAR 1*, National Institute of Standards and Technology, Gaithersburg, MD.

Sadek, F., Main, J.A., Lew, H.S., Robert, S.D., Chiarito, V.P., El-Tawil, S. (2010). *An Experimental and Computational Study of Steel Moment Connections under a Column Removal Scenario*, *NIST TN 1669*, National Institute of Standards and Technology, Gaithersburg, MD.

Figure Captions

Fig. 1. Test setup and instrumentation layout for steel SMF assembly

Fig. 2. (a) WUF-B connection details for steel IMF assembly; (b) RBS connection details for steel SMF assembly

Fig. 3. Photographs of steel IMF assembly test

Fig. 4. Failure mode of steel IMF assembly

Fig. 5. (a) Vertical load and (b) beam axial force versus vertical displacement of center column for steel IMF assembly

Fig. 6. (a) Detailed and (b) reduced models of steel IMF assembly

Fig. 7. Failure mode from detailed model of steel IMF assembly

Fig. 8. Failure mode of steel SMF assembly

Fig. 9. (a) Vertical load and (b) beam axial force versus vertical displacement of center column for steel SMF assembly

Fig. 10. Failure mode from detailed model of steel SMF assembly

Fig. 11. Test setup and instrumentation layout for concrete IMF assembly

Fig. 12. (a) Schematic of concrete assemblies; (b) section properties for IMF assembly; (c) section properties for SMF assembly

Fig. 13. Photograph of concrete SMF assembly in post-ultimate-load position

Fig. 14. (a) Vertical load and (b) beam axial force versus vertical displacement of center column for concrete IMF assembly

Fig. 15. Failure mode of concrete IMF assembly

Fig. 16. (a) Detailed and (b) reduced models of concrete IMF assembly

Fig. 17. Failure mode from detailed model of concrete IMF assembly

Fig. 18. (a) Vertical load and (b) beam axial force versus vertical displacement of center column for concrete SMF assembly

Fig. 19. Failure mode of concrete SMF assembly

Fig. 20. Failure mode from detailed model of concrete SMF assembly

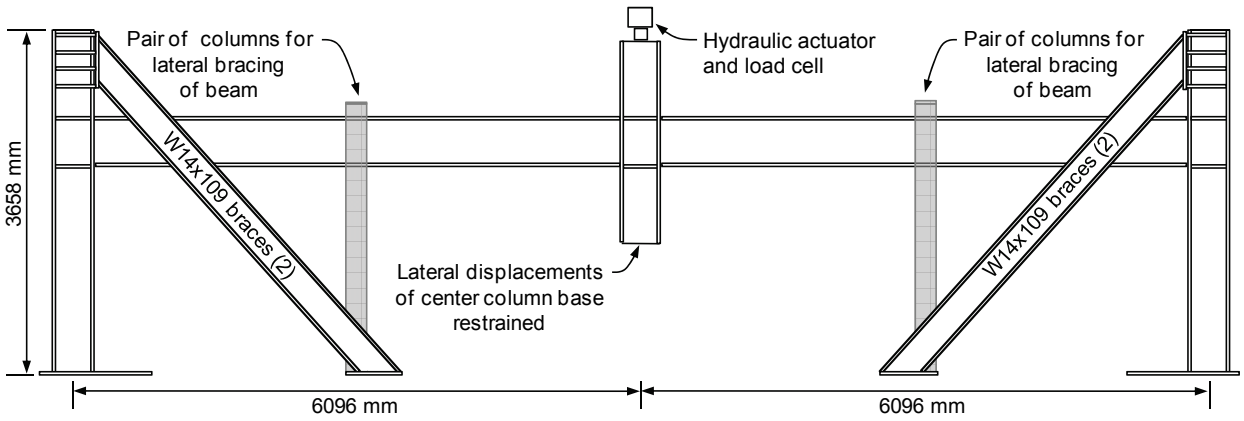

Fig. 1. Test setup and instrumentation layout for steel SMF assembly

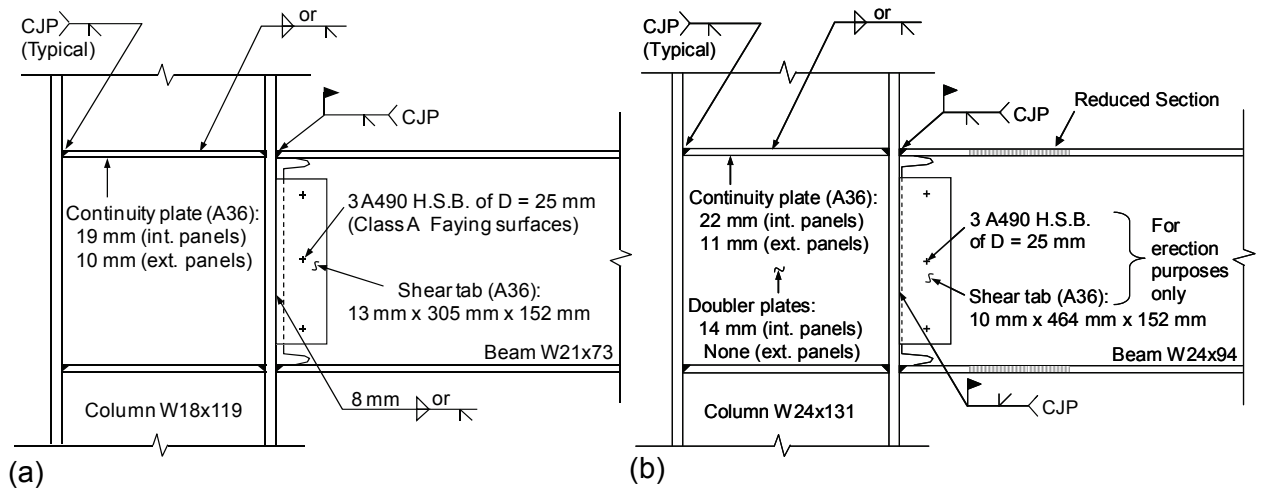

Fig. 2. (a) WUF-B connection details for steel IMF assembly; (b) RBS connection details for steel SMF assembly

Fig. 3. Photographs of steel IMF assembly test

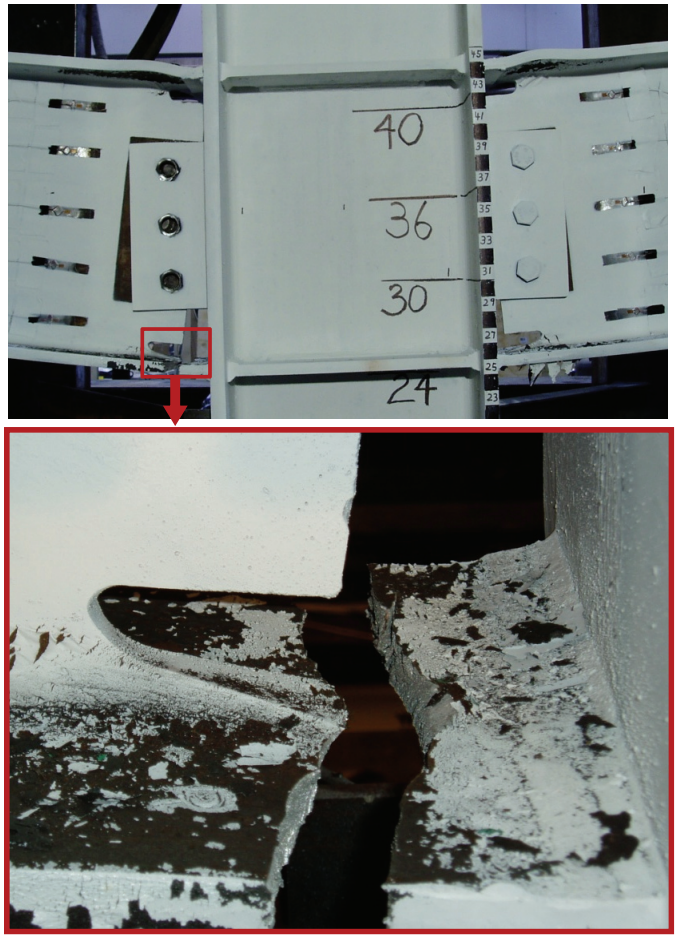

Fig. 4. Failure mode of steel IMF assembly

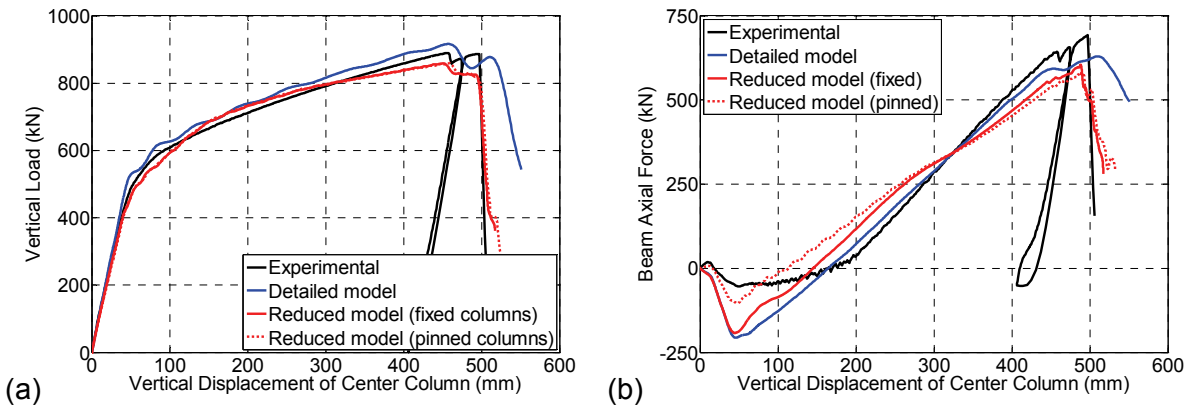

Fig. 5. (a) Vertical load and (b) beam axial force versus vertical displacement of center column for steel IMF assembly

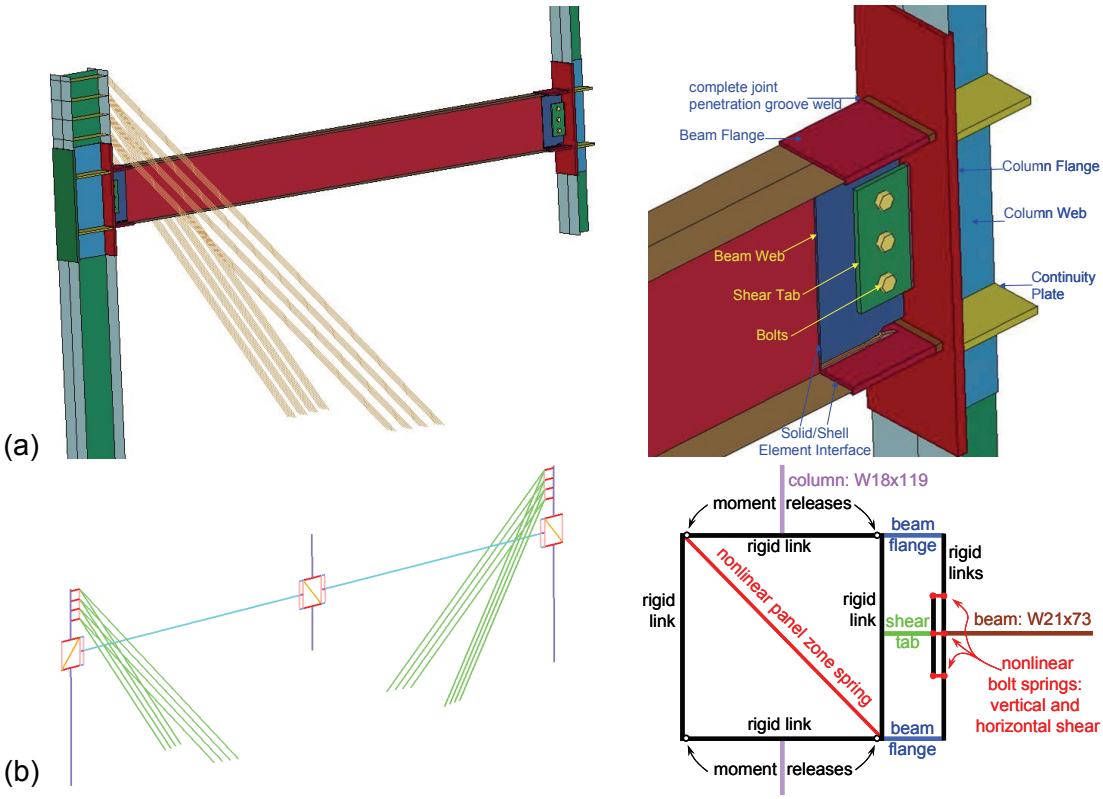

Fig. 6. (a) Detailed and (b) reduced models of steel IMF assembly

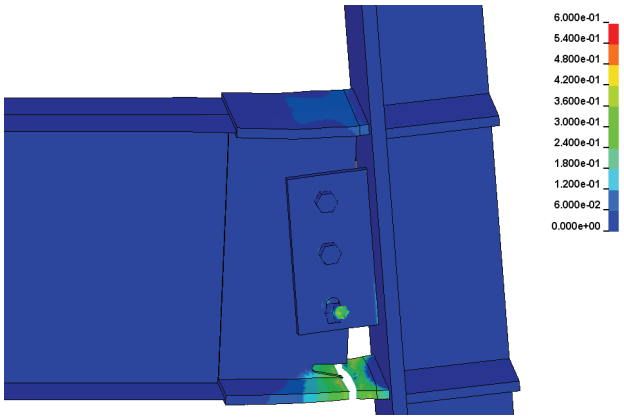

Fig. 7. Failure mode from detailed model of steel IMF assembly

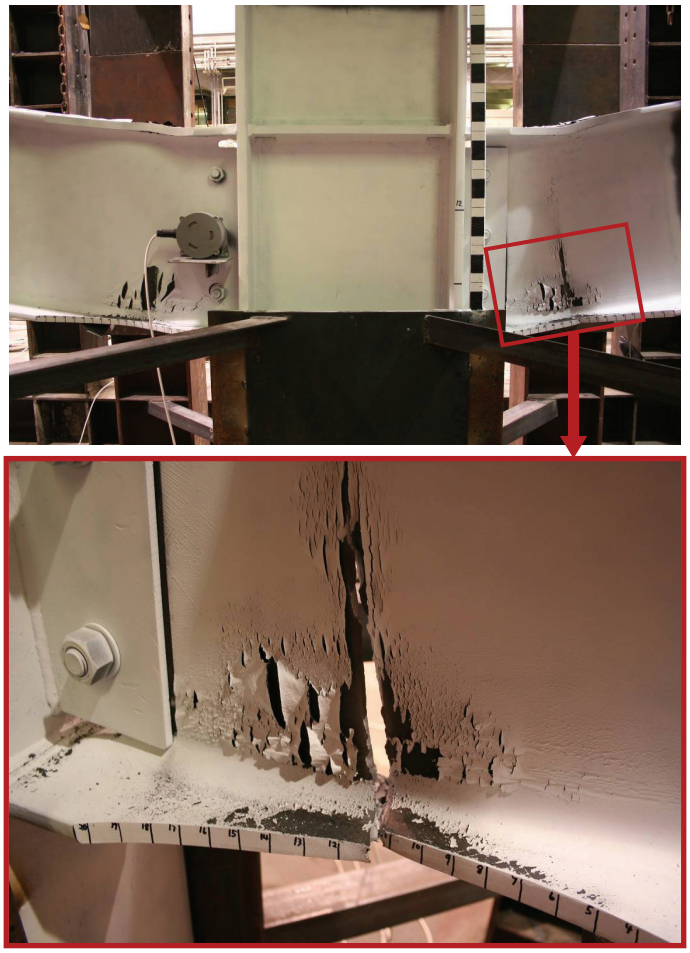

Fig. 8. Failure mode of steel SMF assembly

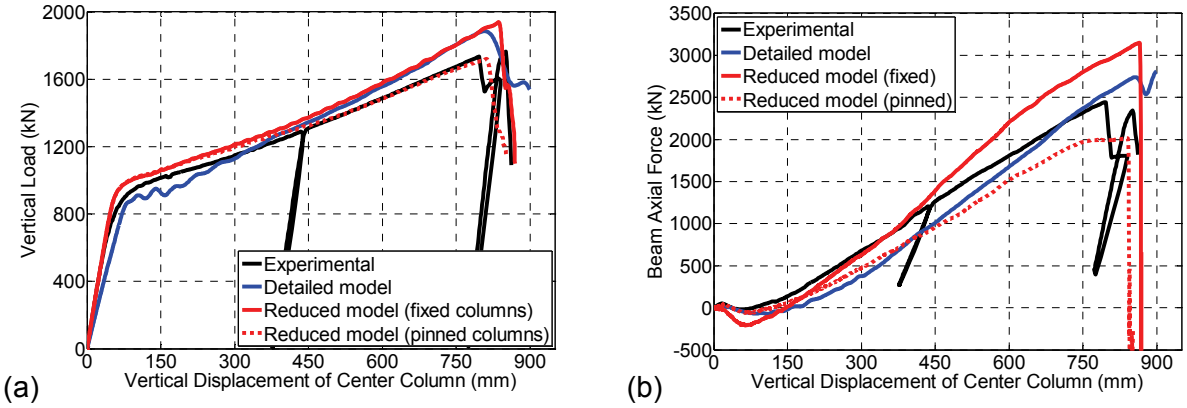

Fig. 9. (a) Vertical load and (b) beam axial force versus vertical displacement of center column for steel SMF assembly

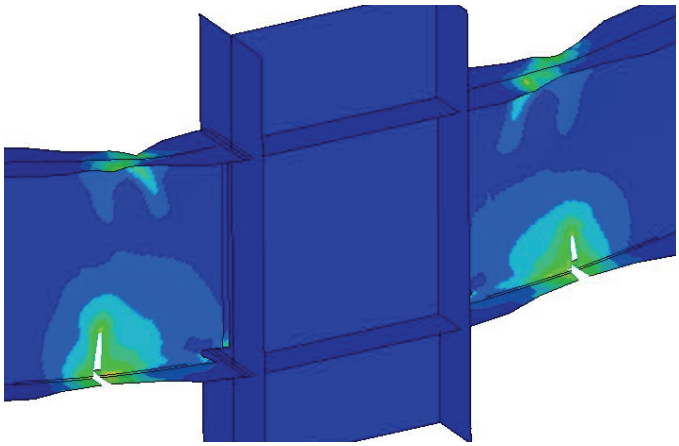

Fig. 10. Failure mode from detailed model of steel SMF assembly

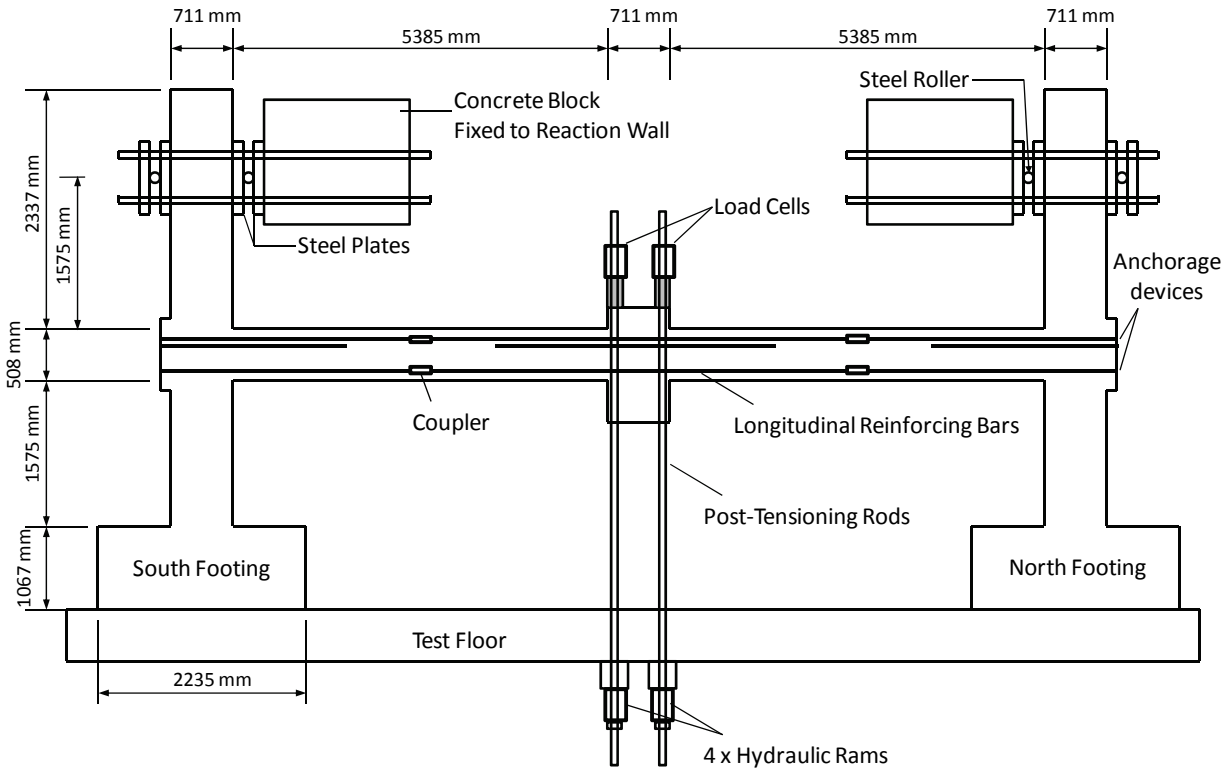

Fig. 11. Test setup and instrumentation layout for concrete IMF assembly

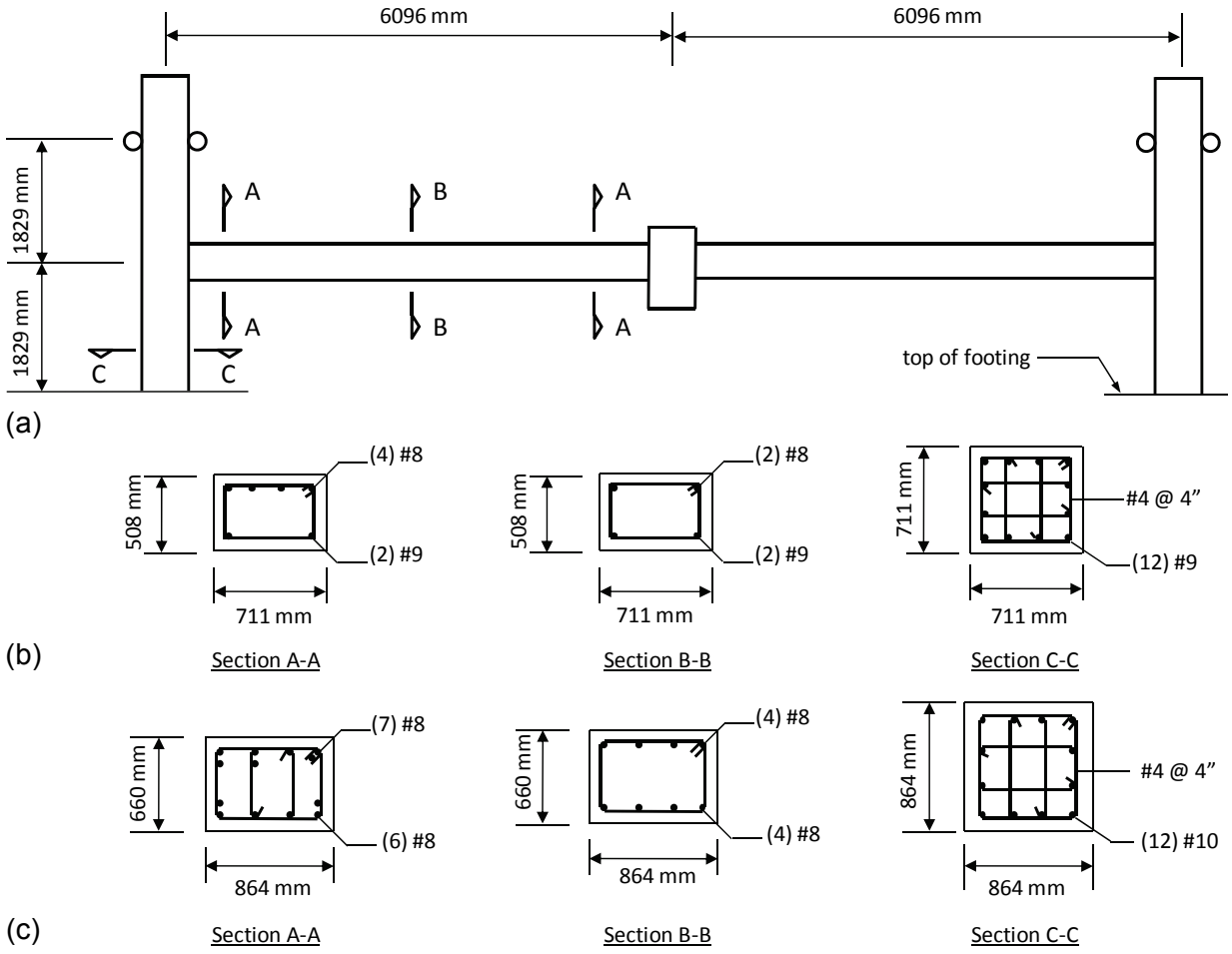

Fig. 12. (a) Schematic of concrete IMF assemblies; (b) section properties for IMF assembly; (c) section properties for SMF assembly

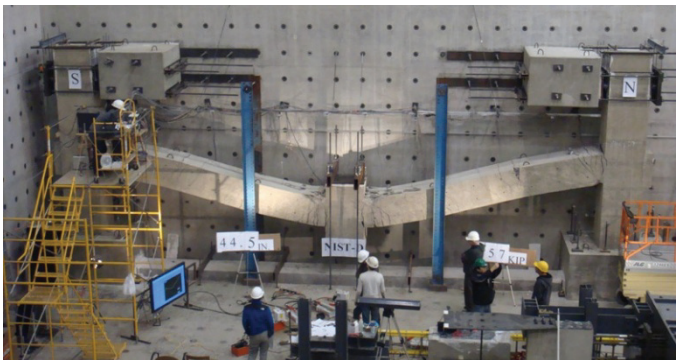

Fig. 13. Photograph of concrete SMF assembly in post-ultimate-load position

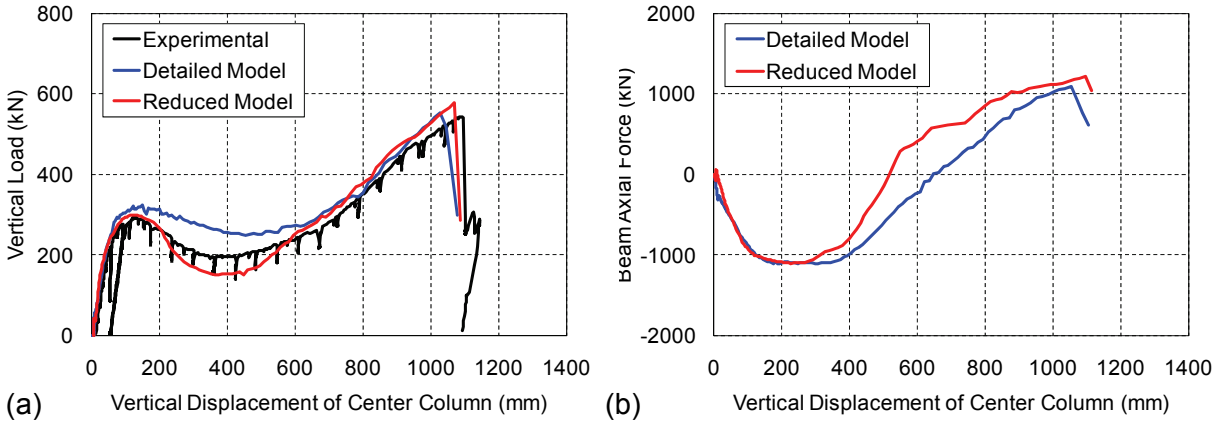

Fig. 14. (a) Vertical load and (b) beam axial force versus vertical displacement of center column for concrete IMF assembly

Fig. 15. Failure mode of concrete IMF assembly

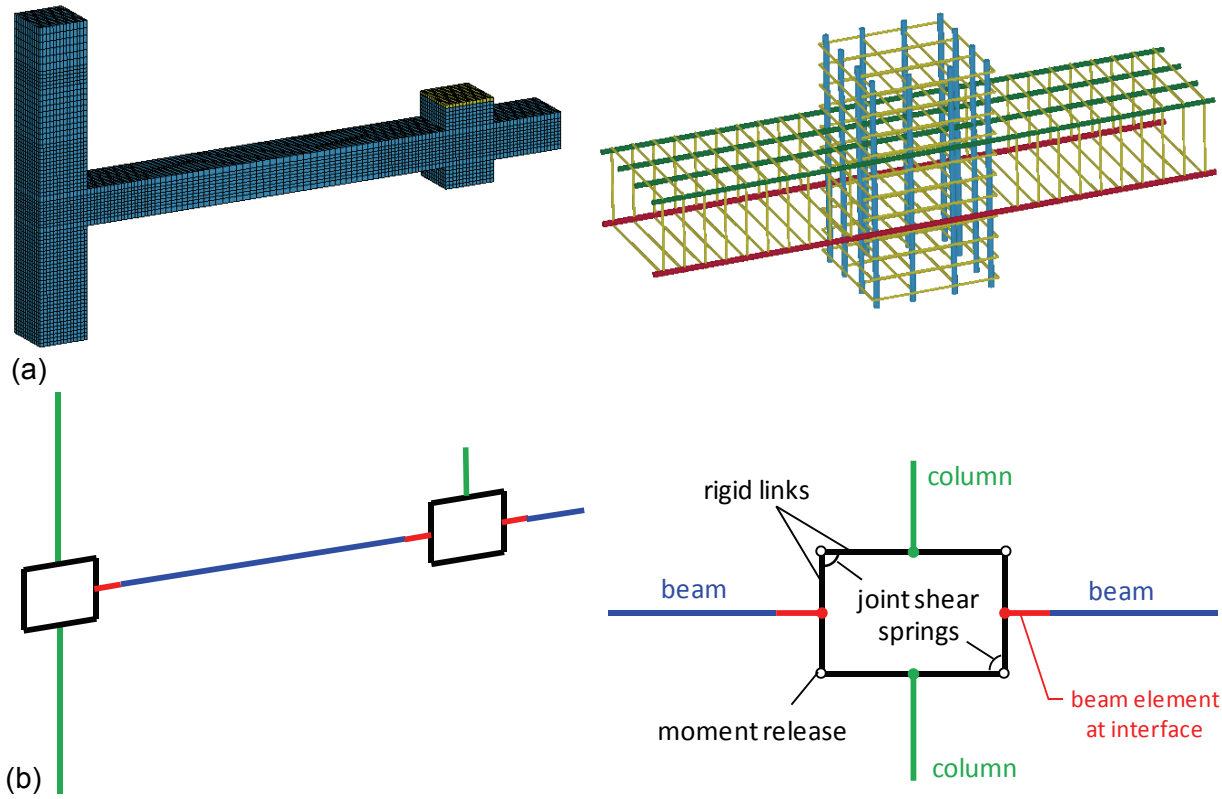

Fig. 16. (a) Detailed and (b) reduced models of concrete IMF assembly

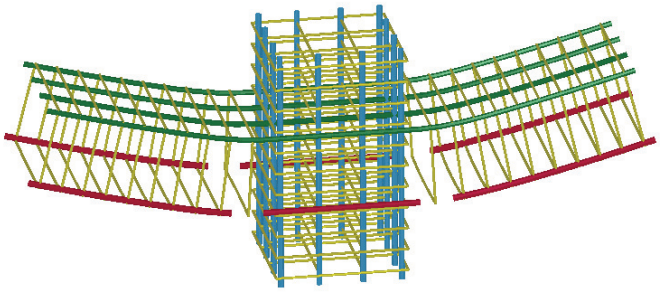

Fig. 17. Failure mode from detailed model of concrete IMF assembly

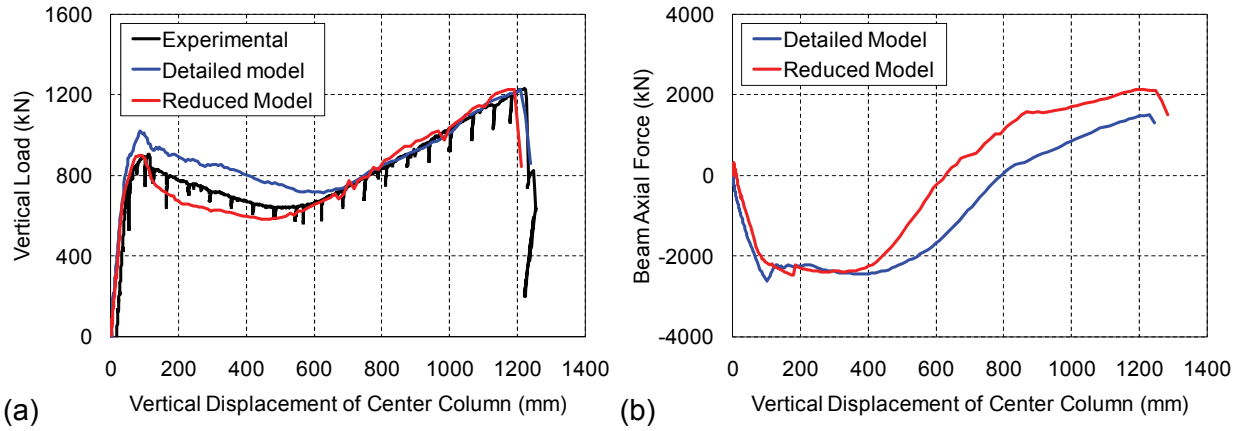

Fig. 18. (a) Vertical load and (b) beam axial force versus vertical displacement of center column for concrete SMF assembly

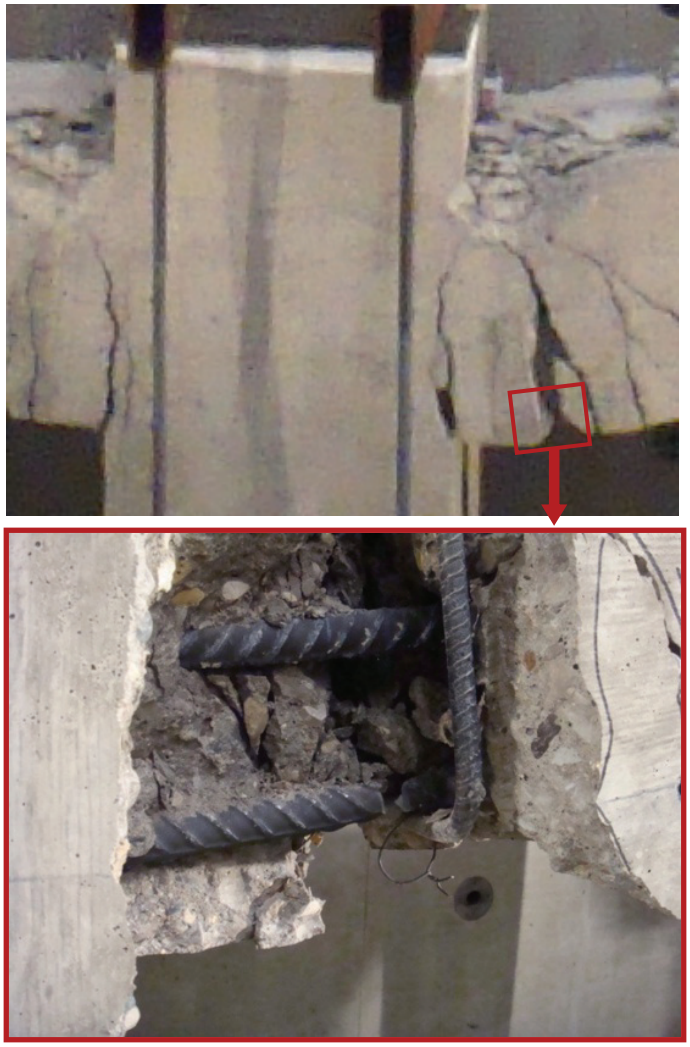

Fig. 19. Failure mode of concrete SMF assembly

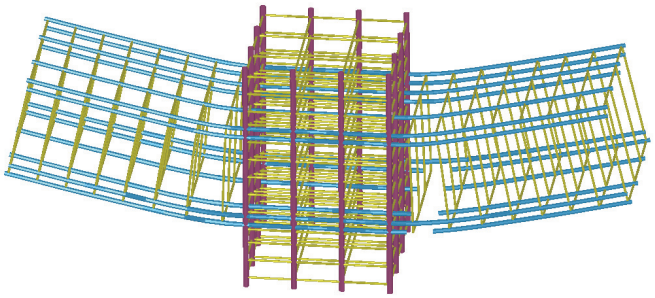

Fig. 20. Failure mode from detailed model of concrete SMF assembly